



HAL
open science

Single-Cell Confinement on Micropatterned Glass Substrates: An AFM Analysis of Cell Height and Topography

Daniele Pedroni, Caroline Gaucher, Halima Alem

► To cite this version:

Daniele Pedroni, Caroline Gaucher, Halima Alem. Single-Cell Confinement on Micropatterned Glass Substrates: An AFM Analysis of Cell Height and Topography. *Langmuir*, 2025, 41 (35), pp.23547-23557. <10.1021/acs.langmuir.5c02609>. <hal-05268931>

HAL Id: hal-05268931

<https://cnrs.hal.science/hal-05268931v1>

Submitted on 13 Jan 2026

HAL is a multi-disciplinary open access archive for the deposit and dissemination of scientific research documents, whether they are published or not. The documents may come from teaching and research institutions in France or abroad, or from public or private research centers.

L'archive ouverte pluridisciplinaire HAL, est destinée au dépôt et à la diffusion de documents scientifiques de niveau recherche, publiés ou non, émanant des établissements d'enseignement et de recherche français ou étrangers, des laboratoires publics ou privés.



Distributed under a Creative Commons CC BY-NC-ND 4.0 - Attribution - Non-commercial use - No Derivative Works - International License

This document is confidential and is proprietary to the American Chemical Society and its authors. Do not copy or disclose without written permission. If you have received this item in error, notify the sender and delete all copies.

Single-Cell Confinement on Micropatterned Glass: an AFM Topographical Profiling

Journal:	<i>Langmuir</i>
Manuscript ID	la-2025-026097
Manuscript Type:	Article
Date Submitted by the Author:	22-May-2025
Complete List of Authors:	Pedroni, Daniele; Institut Jean Lamour, N2EV Gaucher, Caroline; Universite de Lorraine, CITHEFOR EA 3452 Alem, Halima; Universite de Lorraine, Institut Jean Lamour

SCHOLARONE™
Manuscripts

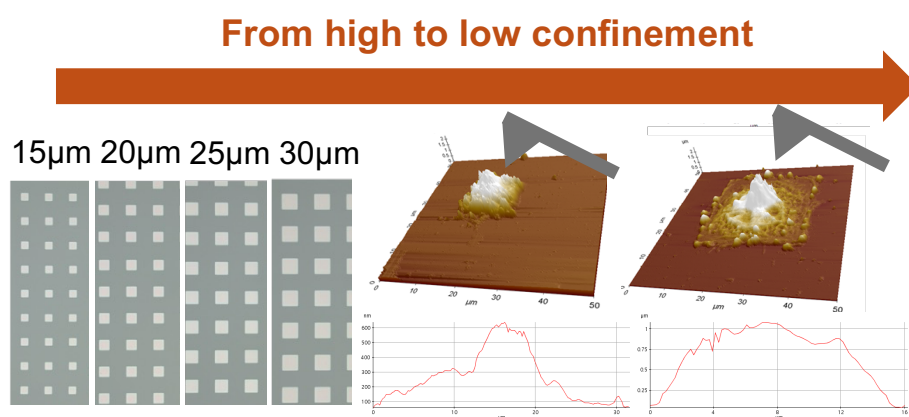
Graphical Abstract

Single-Cell Confinement on Micropatterned Glass: an AFM Topographical Profiling

Daniele Pedroni^{1,2}, Caroline Gaucher² and Halima Alem¹*

¹Université de Lorraine, CNRS, IJL, F-54000 Nancy, France

²Université de Lorraine, CITHEFOR, F-54000 Nancy, France



Confinement modulates cell height and surface roughness. Deep AFM analysis reveals morphological and nanomechanical shifts

Single-Cell Confinement on Micropatterned Glass: an AFM Topographical Profiling

Daniele Pedroni^{1,2}, Caroline Gaucher² and Halima Alem¹*

¹Université de Lorraine, CNRS, IJL, F-54000 Nancy, France

²Université de Lorraine, CITHEFOR, F-54000 Nancy, France

Keywords: Micropatterning, Atomic Force Microscopy (AFM), Endothelial Cells, Cell Topography, Surface Roughness

Abstract

Atomic Force Microscopy (AFM) offers nanometrical resolution for analyzing cellular topography and mechanical properties. However, the inherent irregularity of cell morphology, the different stages of the cell cycle and the inter-cell interaction inside a culture often complicates accurate measurements. To overcome this limitation, we employed micropatterning techniques to standardize cell shape by forcing endothelial cells to adopt a uniform, square configuration. Cells were cultured on microfabricated substrates featuring

1
2
3 square patterns of 10, 15, 20, 25, and 30 μm side. Following silanization and cell seeding,
4
5 individual cells conformed to these defined geometries, permitting consistent AFM scans
6
7 through the entire area of cells. We extracted key topographical parameters, including the
8
9 average and RMS height profiles, root mean square slope (Sdq), as well as higher-order
10
11 statistics such as kurtosis and skewness. A high-pass filter was applied to isolate local surface
12
13 roughness from overall cell shape. Our analysis revealed significant differences in both height
14
15 and roughness parameters between cells confined to smaller *versus* larger patterns, indicating
16
17 that the available adhesion area critically influences cell morphology. Notably, kurtosis and
18
19 skewness metrics further underscored distinct differences in height distribution across the
20
21 various pattern sizes. These findings demonstrate that combining micropatterning with AFM
22
23 provides a robust platform for single-cell studies, offering enhanced reproducibility and deeper
24
25 insights into how controlled cell shape modulates surface properties and cellular function.
26
27
28
29
30
31
32
33
34
35

36 Introduction

37 Characterizing single-cell topography and mechanics is crucial for understanding cellular
38
39 function, but conventional methods struggle with cell-to-cell variability. Atomic Force
40
41 Microscopy (AFM) is a powerful imaging technique that enables high-resolution topographical
42
43 analysis of surfaces at the nanometer scale. Unlike optical and electron microscopy, AFM
44
45 operates by scanning a sharp probe over the sample surface, measuring the interaction forces
46
47 between the tip and the sample^{1,2}. Its various operational modes and the modularity of key
48
49 components, such as the tip shape, have paved the way for the use of AFM in numerous
50
51 biomedical applications^{3,4}. These include the study of the physical and mechanical properties
52
53 of biological elements and biomaterials, such as cells and bacterial membrane⁴⁻⁹, as well as
54
55
56
57
58
59
60

1
2
3 investigations into the nature of interactions between specific components, such as proteins or
4
5 drugs^{10,11}. Moreover, the data collected through AFM have been a useful integration when
6
7 coupled with other forms of microscopy, such as confocal^{12,13}, fluorescence^{14,15}, Raman¹⁶ and
8
9 optical microscopy¹⁷. Traditional bulk analysis methods often overlook cell-to-cell variability,
10
11 making the characterization of single cells an important step for obtaining precise and
12
13 representative data¹⁸. Therefore, the study of single-cell properties may be the answer for
14
15 understanding fundamental biological processes, disease mechanisms, and cell responses to
16
17 external stimuli^{19,20}. AFM has been widely employed for those studies due to its ability to
18
19 provide mechanical characterization at the nanoscale²¹⁻²⁴. The main difficulty remains in single-
20
21 cell isolation and culture on a substrate. To that purpose, multiple techniques have been
22
23 previously employed to isolate and analyze single cells such as microfluidics traps or
24
25 fluorescence activated cell sorting²⁵. Micropatterning, a type of treatment that allows localized
26
27 surface modifications to be created to tune local bio-adhesive potential might be propose to
28
29 isolate one cell from another. Micropatterning is usually achieved by “printing” protein patterns
30
31 on a specific surface using an elastomeric mold, such as PDMS, and then passivating the
32
33 remaining surface with bovine serum albumin^{26,27}, Pluronic f-127²⁸, or polyethyleneglycol-L-
34
35 polylacticacid²⁹. Another possibility is to take advantage of surface chemistry to covalently
36
37 modify its adhesive properties, for example by using silane composites associated with a
38
39 passivating agent like PEG³⁰⁻³². After that, the patterning process can be achieved either by
40
41 photopatterning^{14,33,34} or through sacrificial structures to “mask” localized parts of the surface
42
43 from chemical treatment^{35,36}.
44
45
46
47
48
49
50
51
52
53
54
55
56
57
58
59
60

1
2
3 The goal of this work is to isolate single human umbilical vein endothelial cells (HUVECs)
4 through a micropatterning technique and to take advantage of the regular shape imposed by the
5
6 patterning to perform a full single-cell study of its topographical and volumetric features and
7
8 highlight the changes that occur within the same type of cells by varying the extension of the
9
10 available surface. To achieve this goal, HUVECs will be cultured on of 15 μm , 20 μm , 25 μm ,
11
12 and 30 μm (length of a square side) glass patterns surrounded by passivated, non-adhesive
13
14 surface. These measures have been chosen since, in previous works, single-cell patterning have
15
16 been observed for measures around 30 μm width for different type of cells^{33,34,37-41}, while 15
17
18 μm square size was the smallest dimension where a regular square shape was maintained by the
19
20 patterned cells. In summary, by confining single cells on micro-fabricated islands of defined
21
22 size, we aim to analyze how the available adhesion area affects cell height and surface
23
24 roughness (via AFM). We hypothesize that smaller adhesive areas will induce noticeable
25
26 increases in cell height and changes in topographical distribution.
27
28
29
30
31
32
33
34
35
36
37
38
39

40 **Materials and Method**

41 *Production of Micropatterned glass surfaces*

42
43
44
45
46 The production of the micropatterned glass surface has been performed as in previous
47
48 experiments (Pedroni et al.⁴²). Briefly, a Borofloat glass wafer 2"300 \pm 20/DSP/Ra<1.2nm
49
50 (Siegert Wafer, DE) was treated with oxygen plasma (Tucano plasm a system, Gambetti
51
52 Vacuum Solution, IT) at 200 W for 300 s. After that, the surface was covered with a 5 nm
53
54 aluminium layer using a Kenosistec KS400HR sputtering machine (Kenosistec, IT), then a
55
56
57
58
59
60

1
2
3 resist ARN 7500.18 (Allresist, DE) was spin-coated on the cleaned surface of the sample for
4
5
6 60 s at 5000 rpm and later heated for 60 s at 85°C on a hotplate.
7

8 Electron-beam lithography was performed on the sample using a Raith 150 E-Beam-Writer
9
10 (Raith, DE). Four different patterns were produced, consisting in matrices squares of 15 μm , 20
11
12 μm , 25 μm , and 30 μm side separated by 30 μm from one another. Each pattern contained only
13
14 one type of square, and the different patterns were vertically separated by 5 mm of empty space.
15
16
17 Once the process was concluded, the sample was developed with MF319 developer for 90 s.
18
19

20
21 The glass surface was treated with O₂ plasma (50W, 60s) to be activated prior to being
22
23 inserted inside the glass reactor chamber to perform gas-phase deposition. Then, the chamber
24
25 was put under partial vacuum (7 mbar) for 4 min and 0.4 ml of 2-
26
27 [Methoxy(polyethyleneoxy)propyl]trimethoxysilane (abcr, DE) was aspirated inside the
28
29 chamber through a valve-controlled opening. The sample was kept inside the reactor at 85°C
30
31 for 24 h. After that, it was removed from the chamber, and the excess silane and the resist were
32
33 cleaned through 20 min of ultrasound in isopropanol. The remaining aluminum was removed
34
35 with a further 90 s rinsing in MF319 developer. The micropatterned glass surface was finally
36
37 cleaned with isopropanol and stored at room temperature until observation with reflected
38
39 microscopy (Leica DM80000M) and/or cell seeding.
40
41
42
43
44
45
46
47

48 Cellularization of Micropatterned glass surfaces

49

50
51 Human umbilical vein endothelial cells (PromoCell GmbH, Heidelberg, DE) were cultured
52
53 at 37 °C under 5% CO₂, using endothelial cell growth medium supplied with basal medium and
54
55 supplement mix (Sigma-Aldrich, USA). This supplemented medium contains fetal calf serum
56
57 (2% v/v), endothelial cell growth supplement (0.4% v/v), epidermal growth factor (recombinant
58
59
60

1
2
3 human) (0.1 ng/ml), basic fibroblast growth factor (recombinant human) (1 ng/ml), heparin (90
4
5 $\mu\text{g/ml}$), and hydrocortisone (1 $\mu\text{g/ml}$). All cells used were between passage four and eight, with
6
7
8
9 media exchange every 48 hours.

10
11
12 Micropatterned glass surfaces were immersed for 30 min in a 70% ethanol solution in water,
13
14 rinsed three times in fresh Dulbecco's phosphate buffered saline (PBS, Sigma-Aldrich, USA)
15
16 and seeded with HUVECs at 10^4 cells/cm² in supplemented medium. Cellularized samples
17
18 were then placed at 37 °C in an incubator under 5% CO₂ for 6 before being were rinsed with
19
20 PBS and fixed for 20 min with 4% m/v paraformaldehyde solution in PBS. Cellularized
21
22 micropatterned glass surfaces were finally stored in PBS at 4°C until analysis.
23
24
25
26

27 *Morphological analysis of cells*

30 *Contrast phase observation*

31
32 Cellularized micropatterned glass surfaces have been observed in phase contrast mode with
33
34 a ZEISS AX10 inverted microscope equipped with and Axiocam 202 mono. The software
35
36 employed for the imaging were the LAS software for the reflected microscopy and ZEN 3.1 for
37
38 the inverted microscopy.
39
40
41

42 *Topographic and volumetric analysis*

43
44
45 Prior to the experiment, the sample was dried by sequential immersion in progressive ethanol
46
47 solutions. Briefly, the PBS was removed, and the surface was immersed for 5 minutes in a 25%
48
49 ethanol solution in distilled water, which was later removed and substituted with a solution of
50
51 50% ethanol in distilled water for 5 minutes. The procedure was repeated for a 75%
52
53 ethanol/distilled water solution and 100% ethanol, after which the sample was put under partial
54
55 vacuum (7mbar) for 30 minutes.
56
57
58
59
60

1
2
3 The dried sample was then placed inside the Park Systems NX10 (Park Systems, Kr) Atomic
4 Force Microscope, and multiple single-cell scans were taken for each type of pattern using Non-
5 Contact Mode (NCM) with an OMCL-AC160TS 10M Non-Contact Cantilever from the same
6 supplier.
7
8
9
10
11
12

13 The scans were acquired on a 50 μ m side square surface containing a single patterned cell
14 with a 256-square-pixel resolution and a resonance frequency between 242 and 247Hz, with a
15 scan rate of 10-20Hz on the cells. The images were observed using XEI software (Park Systems,
16 Kr) and flattened using a first-degree polynomial.
17
18
19
20
21
22

23 *Statistical Analysis*

24
25 Using the XEI software, the average profile of a patterned cell was acquired for each scan. A
26 “profile” is the plot of every height measurement of a single linear scan, while the “average
27 profile” is the plot of the mean of every measurement on the Y-axis, given a linear scan on the
28 X-axis. The direction and length on X and Y are arbitrary, and the resulting area was set to be
29 the closest square on the X-axis (scan length [μ m]) to include any height measurements outside
30 the pattern whenever present.
31
32
33
34
35
36
37
38
39
40
41
42

43 The resulting average profiles for n=10 scans for each class of pattern dimension were
44 exported to Excel software, where the mean and standard error were calculated for each point
45 on the X-axis.
46
47
48
49

50 Area under curve (AUC) was extracted from each profile by integration using the trapezoidal
51 rule :
52
53
54
55
56
57
58
59
60

$$\sum_{i=1}^{n-1} \frac{f(x_i) + f(x_{i+1})}{2} \cdot (x_{i+1} - x_i)$$

As a mean to compare the different cell profiles, the AUC of each class of dimension have been compared through Kruskal-Wallis ANOVA followed Dunn's test for pairwise comparisons (OriginPro software). The null hypothesis was rejected for $p < 0.05$. A non-parametric test was chosen after demonstrating the non-normality of the $25 \mu\text{m}$ size distribution through Shapiro-Wilk normality test.

Using the surface analysis function of the XEI software, it was possible to calculate root mean square height (Sq), arithmetic mean height (Sa), kurtosis (Sku), skewness (Ssk), maximum height of the peaks (Sk), and root mean square slope (Sdq).

To study the surface roughness, the scans were filtered through a high-pass filter (kernel = 3) to eliminate the "slow" changes in topography. This expedient allowed for the removal of the actual shape of the cell, leaving only the localized surface texture to be considered. This approach made it possible to analyze the root mean square roughness (RMS Roughness), the arithmetic average roughness, the root mean slope roughness, the core void volume, and the core material volume.

The Sq and the RMS Roughness are measured as follows:

$$S_q = \sqrt{\frac{1}{A} \iint_A z^2(x,y) \, dx \, dy}$$

The height is indicated with "z" and the flat surface area on which the measurement is conducted with "A". Sq and RMS roughness are useful to be compared to the (Sa) and

1
2
3 arithmetic mean roughness, since it gives an increased importance to high peaks and valley.

4
5
6 This value is amplified by its square elevation, while the arithmetic parameters are measured
7
8 as it follows:
9

$$S_a = \frac{1}{A} \iint_A |z(x,y)| \, dx \, dy$$

10
11
12
13
14
15
16 Kurtosis of topography height distribution, S_{ku} , is a parametric measurement of the steepness
17
18 of the height distribution of a surface⁴³. By convention, a $sku > 3$ indicates a leptokurtotic
19
20 behaviour of the height distribution, with a sharp peak indicating a high concentration of height
21
22 measurement around a single parameter, while a $sku < 3$ indicates a platikurtotic behaviour, and
23
24 therefore a more distributed number of the height measurements through the entire vertical
25
26 projection of the structure.
27
28
29
30
31
32

$$S_{ku} = S_q^{-4} \left(\frac{1}{A} \iint_A z^4(x,y) \, dx \, dy \right)$$

33
34
35
36
37
38
39
40
41
42 The skewness (s_{sk}) of the height distribution is a statistical parameter that describes the
43
44 asymmetry of the surface height values relative to the base surface and gives an indication of
45
46 how high the average height is compared to the total height span of the analyzed surface.
47
48
49
50

$$S_{sk} = S_q^{-3} \left(\frac{1}{A} \iint_A z^3(x,y) \, dx \, dy \right)$$

Sp is the maximum height of the peaks, which is the maximum height value registered on any given cell at any scan.

The Root Mean Square Slope (s_{dq}) is a value used to assess regularity of a surface by measuring the average slope angle (expressed in radian) on a given area, and is expressed as it follows:

$$S_{dq} = \sqrt{\frac{1}{A} \iint_A \left[\left(\frac{\partial z(x,y)}{\partial x} \right)^2 + \left(\frac{\partial z(x,y)}{\partial y} \right)^2 \right] dx dy}$$

Where A is the given flat surface area, $z(x,y)$ the function of the surface while $\left(\frac{\partial z(x,y)}{\partial x}\right)^2$ and $\left(\frac{\partial z(x,y)}{\partial y}\right)^2$ are the partial derivatives of the function $z(x,y)$ on both axis.

Core void volume (VVC') and core material volume (VMC') are both volume-based measurements that rely on the concept of the Abbot-Firestone curve, which shows the percentage distribution of the volume relative to the height of the surface measurement. Conventionally, the term "core" refers to the portion of the curve between 10% and 80%, thus excluding the deepest pits and the highest peaks relative to the actual volume measured.

VVC' and VMC' represent, respectively, the void and the material volume within the core area of the roughness of each cell. Both parameters are calculated on the filtered scans.

All these parameters were measured on the cell surface, taking advantage of the square shape imposed by the chemical patterning to avoid including external, unrelated measurements in the computation.

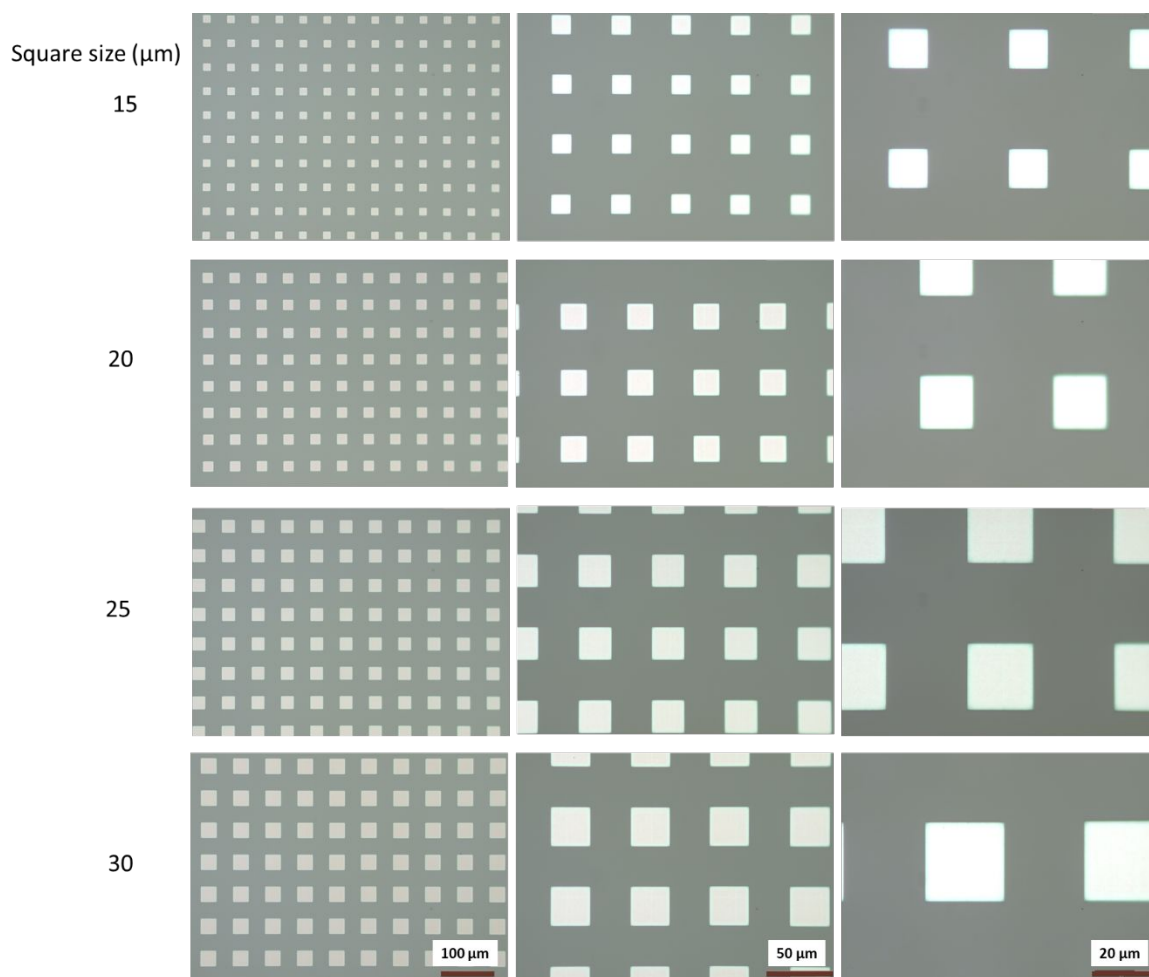
1
2
3 For each size class, $n= 10$ cells for each class of dimension were scanned, resulting in the
4
5 same number of average profile assessments and measurements for each of the listed roughness
6
7 parameters. The experimental conditions allowed individual cells to be scanned and enabled
8
9 analysis of the full surface of each cell.
10
11

12
13 Resulting data were compared using Kruskal-Wallis ANOVA followed Dunn's test for
14
15 pairwise comparisons (OriginPro software). The null hypothesis was rejected for $p<0.05$.
16
17
18
19

20 **Results and Discussion**

21

22
23 After lithography, the resulting micrometrical structures have been observed by contrast
24
25 phase microscopy (Figure 1). E-beam lithography is a well-known technique for producing
26
27 micro and nanometrical features on various types of conductive surfaces and has a long history
28
29 of application in the molecular patterning either by local modification of the surface parameters
30
31 or through sacrificial structures^{35,44-46}. While the use of this machine is commonly indicated
32
33 for conductive surfaces such as silicon, it can be employed on insulating surfaces, such as glass,
34
35 as long as they are covered with a layer of conductive material like aluminum, chromium or
36
37 copper^{47,48}. Figure 1 observations validate the microfabrication process with squares of desired
38
39 dimension and spacing.
40
41
42
43
44
45
46
47
48
49
50
51
52
53
54
55
56
57
58
59
60



35
36
37
38
39
40

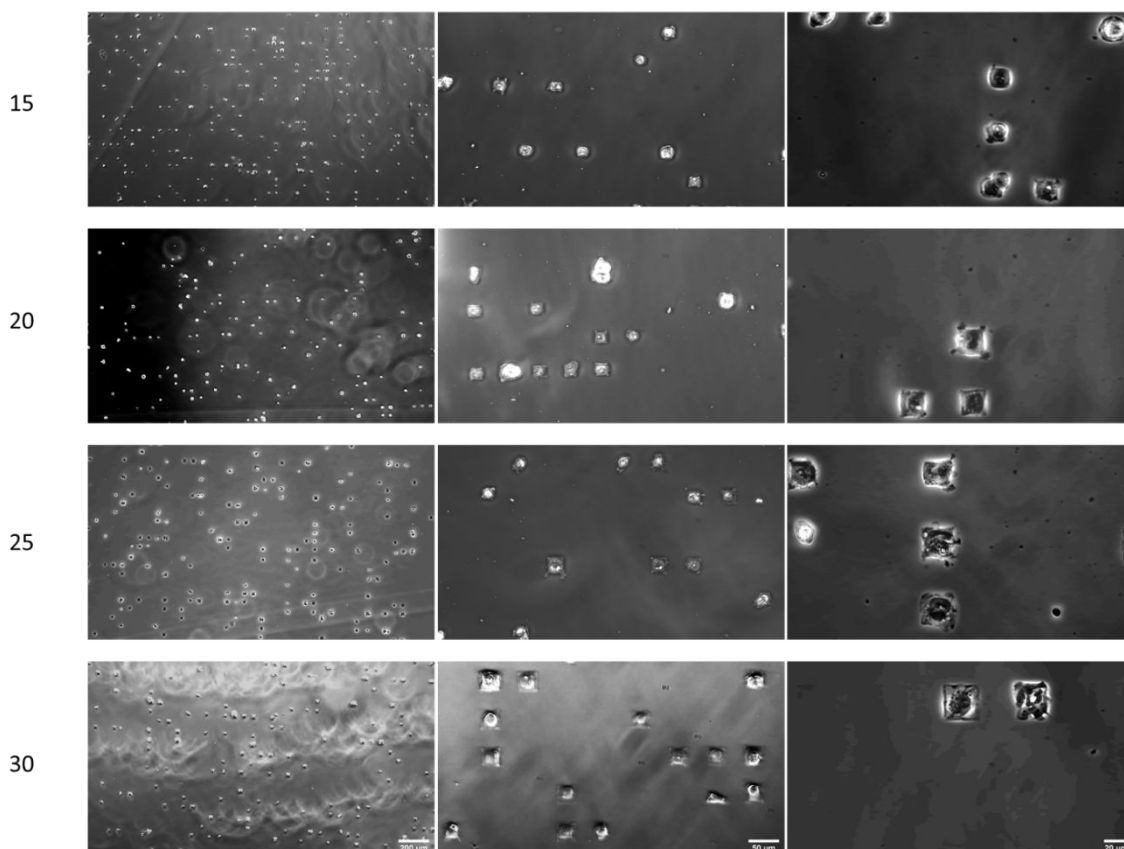
Figure 1. Representative images of glass resist structures with different square sizes spaced by 30 μm . Images acquired with a reflected light microscope (Leica DM80000M).

41
42
43
44
45
46
47
48
49
50
51
52
53
54
55
56
57
58
59
60

Six hours after seeding on silanized glass surface, cells display the same shape and spacing as the sacrificial structures for all classes of dimension (Figure 2). Our observation confirmed the results obtained by other studies, that reached the same results with patterns of comparable sizes and shapes and with different types of cells^{33,34,37-41}, while the presence of multiple cells has been noted on square patterns of 60 μm size⁴⁹. Moreover, it was also shown that other shapes such as linear or rectangular pattern larger than 30 μm would occasionally host more than one cell at a time⁵⁰, while this does not seem to occur with squares of 30 μm size as we observed.

1
2
3 Indeed, in our experiment, each cellularized square seemed to host only one cell, and none of
4
5 the microscope observation or AFM scan indicate otherwise. Finally, the square spacing of 30
6
7 μm , chosen to minimize interactions between cells located on different squares, as observed by
8
9 others in between 20 μm ³⁸ and 30 μm ⁵¹, is enough to maintain cell isolation after 6 h.
10
11
12
13
14

15 Square size (μm)



46
47 **Figure 2.** Representative images of HUVECs on micropatterned glass surfaces 6 h after seeding
48
49 on different square sizes spaced by 30 μm . Images acquired with a phase contrast microscope
50
51 (ZEISS AX10 equipped with and Axiocam 202 mono)
52
53

54
55 After six hours, cells were fixed in paraformaldehyde, and the surface was dehydrated
56
57 through immersion into progressive ethanol. Both procedures are known to preserve cell shape
58
59
60

1
2
3 and topography^{52-54 55}. Then, cells were individually scanned by AFM. Each scan included an
4 area of a $50\mu\text{m} \times 50\mu\text{m}$ area and a single patterned cell regardless of its dimension.
5
6 Consistently with phase-contrast microscope observations (Figure 2), all scanned cells assume
7
8 the shape of one of the 4 square patterns present on the micropatterned glass surface (**Error!**
9
10
11 **Reference source not found.** a, b, c, d). For each scan, the average profile was extracted through
12
13
14 the entire length of each scanned cell. The “profile” is the graphical representation of the heights
15
16
17 of a structure scanned along a line, while the “average profile” is the graph resulting from the
18
19
20 mean of every height measurement on the same Y-axis.
21
22
23
24
25
26
27
28
29
30
31
32
33
34
35
36
37
38
39
40
41
42
43
44
45
46
47
48
49
50
51
52
53
54
55
56
57
58
59
60

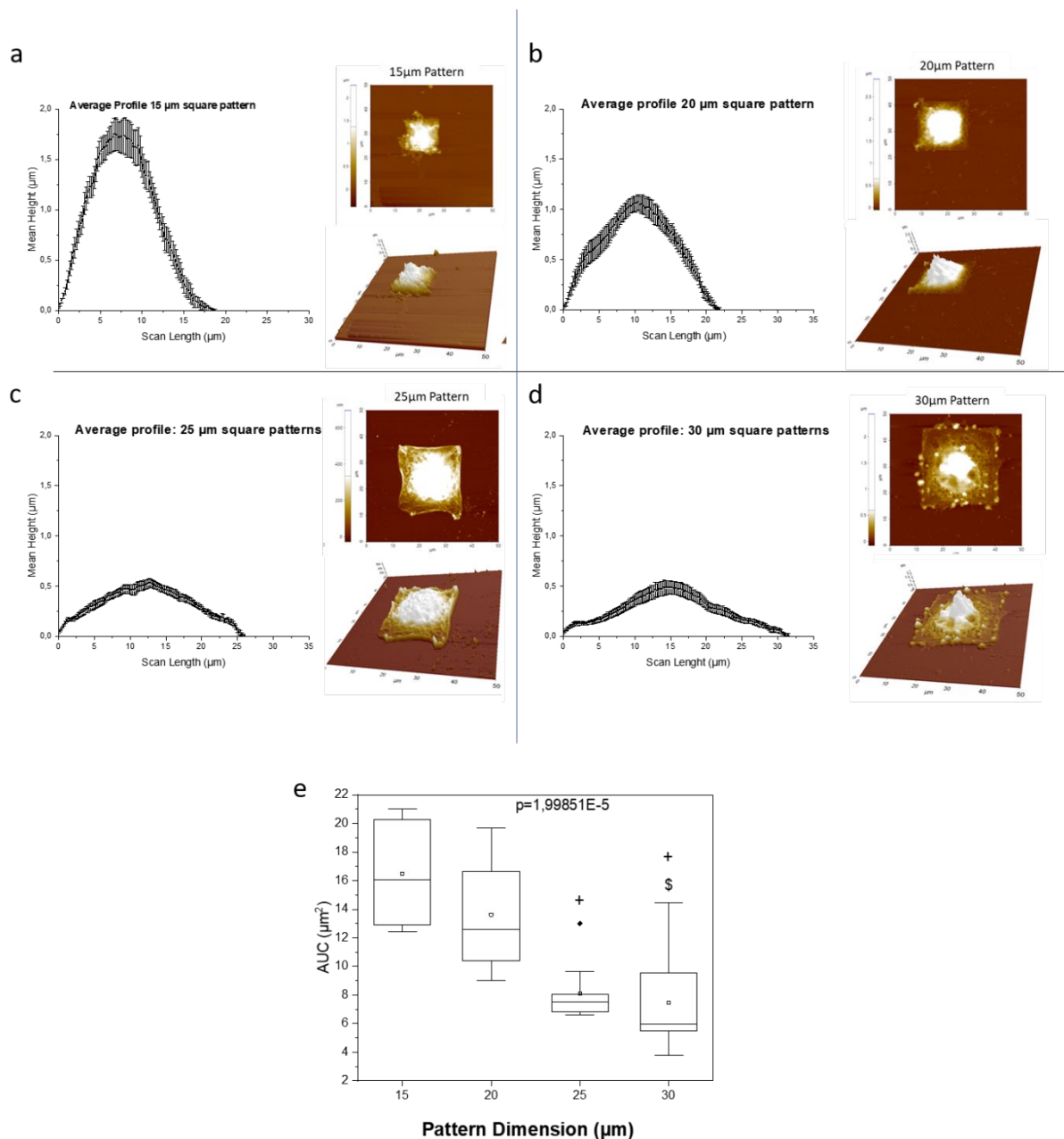


Figure 3. Average height profile of HUVECs and 2d and 3d topography maps of HUVECs fixed patterned glass. Acquisition made with Park Systems AX10. Images were flattened with XEI software (Park Systems, Kr) ; (a) 15 μm square, (b) 20 μm square; (c) 25 μm square; (d) 30 μm square

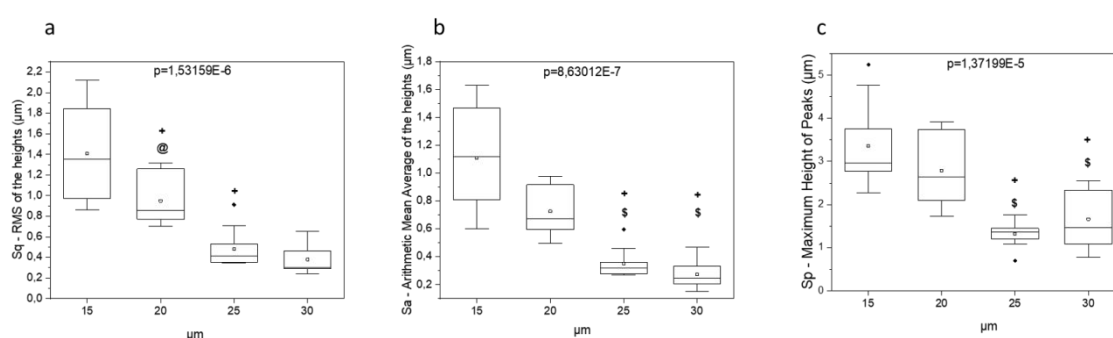
The height profile of different cells has been measured in previous works and is usually represented as either the cross-section, the maximum height, or the average of multiple profiles

1
2
3 sampled from different cells^{16,24,56–59}. The reason why the single scan line is used as the main
4
5 representation of the cell profile is likely due to the irregular and rather unpredictable shape of
6
7 the cells in static conditions, which would result in parameters like the average profile being
8
9 used exclusively for limited sections of the cell. Performing a scan on a square (or rectangular)
10
11 patterned cell would guarantee the possibility to observe the average profile of the entire cell
12
13 through its total surface while minimizing the risk of background noise in the data.
14
15
16
17

18 **Error! Reference source not found.** (a, b, c, d) presents the resulting average profile of 10
19
20 cells scanning per pattern dimension to decipher which areas of the cell show the highest
21
22 variation. There is an evident difference between the shapes of the profiles both along the X-
23
24 axis (the scan length) and the height of the different curves. As observed on the 15 μm and 20
25
26 μm , the reduction of the available surface for colonization brings the cells to adopt higher profile
27
28 and overall, a higher average height compared to cells distributed on larger 25 μm and 30 μm
29
30 areas. Specifically, while there is an evident difference in average height of cells seeded on 10
31
32 μm , 20 μm , and 25 μm or 30 μm side squares, there is no difference between 25 μm and 30 μm .
33
34 The measurement of the AUC through the integration of the curves allows for a comparison
35
36 between the different dimension, as it can be considered the average section area for the patterned
37
38 cells. In Figure 3e, statistical analysis confirms an overall difference between 15 μm square
39
40 patterned cells and the 25 μm and 30 μm classes, suggesting that a limitation of the adhesive
41
42 surface might cause an higher average area of the section and therefore an higher volume
43
44 concentration per unit of length compared to cells with larger surface to colonize. As confirmed
45
46 by the qualitative observations, there seems to be no difference in the average surface area
47
48 between cells patterned on 25 μm and 30 μm square. In this specific case, while there is a
49
50
51
52
53
54
55
56
57
58
59
60

1
2
3 difference in the length of the cells along the scan axis due to the different dimensions of the
4
5
6 pattern, there is little difference between the curves.
7
8
9

10
11 Full height parameters such as RMS, arithmetic mean average and maximum height (Figure
12
13 4 a, b and c) are consistent in showing a significant difference in the vertical measurements of
14
15 cells on 10 μm or 15 μm compared to those cultured in 25 and 30 μm squares suggesting that a
16
17 10 μm change in a pattern dimension is enough to generate a significant difference in height.
18
19 The highest peak is an important parameter for assessing how cell height changes depending
20
21 on the amount of available surface, it must be noted that this kind of absolute measurement is
22
23 the most prone to machine glitches or sample contamination. Despite these premises, Figure 4
24
25 c shows that maximum height changes significantly in the range of 20 to 25 μm in dimension,
26
27 while measurements over a similar gap (25-30 μm and 15-20 μm) showed no significant
28
29 difference.
30
31
32
33
34
35
36
37
38
39
40



41
42
43
44
45
46
47
48
49
50
51 **Figure 4.** Surface analysis of HUVEC (a) Root mean square of the heights; (b) Arithmetic mean
52
53 average of the heights; (c) Maximum height of the peaks. Statistical analysis and graphs are
54
55 made with Kruskal-Wallis ANOVA followed by Dunn's test for multiple comparisons
56
57
58
59
60

1
2
3 (OriginPro) with $^+p < 0.05$ versus 15 μm and $^{\$}p < 0.05$ versus 20 μm and $^{\text{@}}p < 0.05$ versus 30
4
5
6 μm .

7
8
9 Then deeper in height investigation, the kurtosis value of height distribution (Figure 5a)
10 indicates that cells patterned on 30 μm showed a significantly higher value compared to those
11 patterned at 15 μm and 25 μm , while no difference with the distribution of cells patterned on 20
12
13
14
15
16
17 μm was observed. More specifically, while height distributions of cells patterned on 15 μm and
18
19
20
21
22
23
24
25
26
27
28
29
30
31
32
33
34
35
36
37
38
39
40
41
42
43
44
45
46
47
48
49
50
51
52
53
54
55
56
57
58
59
60

Then deeper in height investigation, the kurtosis value of height distribution (Figure 5a) indicates that cells patterned on 30 μm showed a significantly higher value compared to those patterned at 15 μm and 25 μm , while no difference with the distribution of cells patterned on 20 μm was observed. More specifically, while height distributions of cells patterned on 15 μm and 25 μm were slightly platykurtic ($Sku < 3$) with a flatter height distribution, the 30 μm patterned cells exhibited kurtosis values mostly concentrated around leptokurtic ($Sku > 3$) levels, signifying that the height measurements were more concentrated around similar values. This measurement becomes useful when applied over the full extent of cell, as it provides a rough indication of the distribution of cell volume over a known surface. When compared with other topographical parameters, it enables the assessment of various hypotheses regarding the height distribution among different subjects. For example, while the kurtosis values of the 20 μm and 30 μm patterned cells were not significantly different, both RMS height and average height comparisons between the same patterns rejected the null hypothesis, suggesting a significantly different height between cells patterned on 20 μm and those on 30 μm . These two parameters suggest that while cells patterned on a larger surface tend to have a concentration of values in the lower heights (a flatter base with sharp and steep peaks), cells patterned on smaller dimensions exhibit a rapid increase in height, leading to a flatter top. However, this assumption does not hold for the intermediate pattern dimensions of 15 μm and 25 μm . To validate the previous observations about the difference in steepness for the height distribution among the different classes of dimension, the RMS slope for the entire cells have been considered (Figure

5c). This measurement considers the variation in angle between subsequent measurement, and results in the rejection of the null hypothesis when comparing 15 μm patterned cells with the 25 μm and 30 μm patterns. These results are also consistent with height-related measurements in Figure 6. Surface analysis of HUVEC (a) Root mean square roughness; (b) Arithmetic mean roughness; (c) Root mean slope roughness; (d)VMC – Core material roughness; (e) VVC’ Void Core Volume Roughness. Statistical analysis and graphs are made with Kruskal-Wallis ANOVA followed by Dunn’s test for multiple comparisons (OriginPro) with $^+p < 0.05$ versus 15 μm and $^{\$}p < 0.05$ versus 20 μm and $^{\textcircled{a}}p < 0.05$ versus 30 μm . 4 (a, b) and show a correlation between both the overall shape slope and cell height.

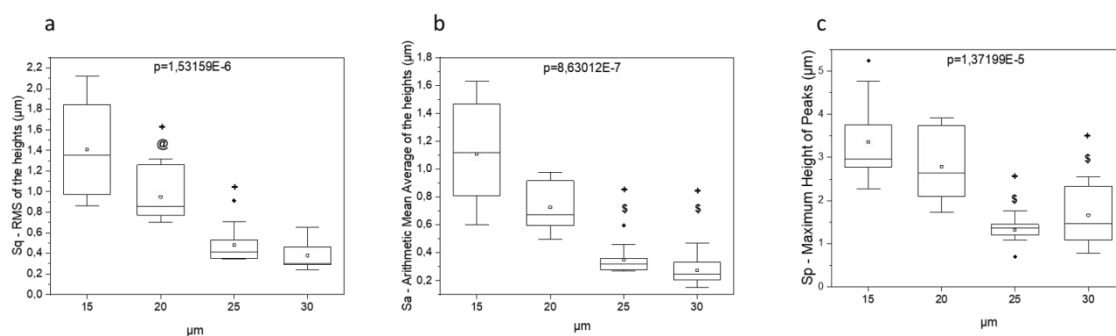


Figure 5. Surface analysis of HUVEC (a) Kurtosis of the height distribution; (b) Skewness of the height distribution; (c) Root mean square slope for the full cell. Statistical analysis and graphs are made with Kruskal-Wallis ANOVA followed by Dunn’s test for multiple comparisons (OriginPro) with $^+p < 0.05$ versus 15 μm and $^{\$}p < 0.05$ versus 20 μm and $^{\textcircled{a}}p < 0.05$ versus 30 μm .

1
2
3 To evaluate cell surface roughness, a high-pass filter was used to remove the “slow”
4 variations in height associated with the actual shape of cells, allowing isolation of only the
5
6 “fast” high-frequency variations associated with surface roughness.
7
8
9

10
11 In the literature, previous observations on cell roughness were made through sampling
12 different parts of the cells^{60–63}, due to experimental necessity, limitations of the equipment or
13 the lack of a regular cell shape, but nonetheless, the results showed that cell roughness could be
14 used as an indicator of cell status, such as oxidative stress⁶⁰ and the mechanical properties of
15 the membrane⁶¹ or the substrate⁶³.
16
17
18
19
20
21
22

23
24 Figure 6 (a, b) shows the average and RMS roughness for each class of dimension,
25 highlighting that in both cases, the only significant difference was found between 15 μm
26 patterns and the 25–30 μm ones, while the 20 μm patterned cells showed no difference with any
27 of the other groups.
28
29
30
31
32

33
34 In **Error! Reference source not found.** (d, e) displays all the core-related values, with “core”
35 indicating the portion of the cell surface within the range between 10%–80% of the total
36 measured height (from the lowest valley to the highest peak). This definition derives from the
37 concept of the Abbott-Firestone curve, or Material Ratio Curve (MRC), which represents the
38 cumulative fraction of the surface area below a certain relative height. It is calculated through
39 the integration of the distribution of measured surface heights and provides important insights
40 into the sample topography. The parameters considered were the Core Material Volume
41 (VMC’) and Core Void Volume (VVC’) the of cells in relation to their surface roughness. As
42 observed, while the data distribution for cells patterned pattern between 15 μm and 25 μm
43 squares showed no significant differences between one another, the 30 μm patterned cells
44
45
46
47
48
49
50
51
52
53
54
55
56
57
58
59
60

surfaces exhibited both a higher surface core volume and a higher VVC' compared to all the other categories. This result aligns with the kurtosis values (**Error! Reference source not found.** b), which revealed a higher concentration of values (expressed as $Sku \gg 3$) compared to most of the other categories, a significantly lower height (Figure 4 a, b) and slope (Figure 5 c), and a visibly lower profile compared to the 10 μ m and 20 μ m patterns (**Error! Reference source not found.** a, b). The roughness parameters were consistent with all other categories except for 15 μ m.

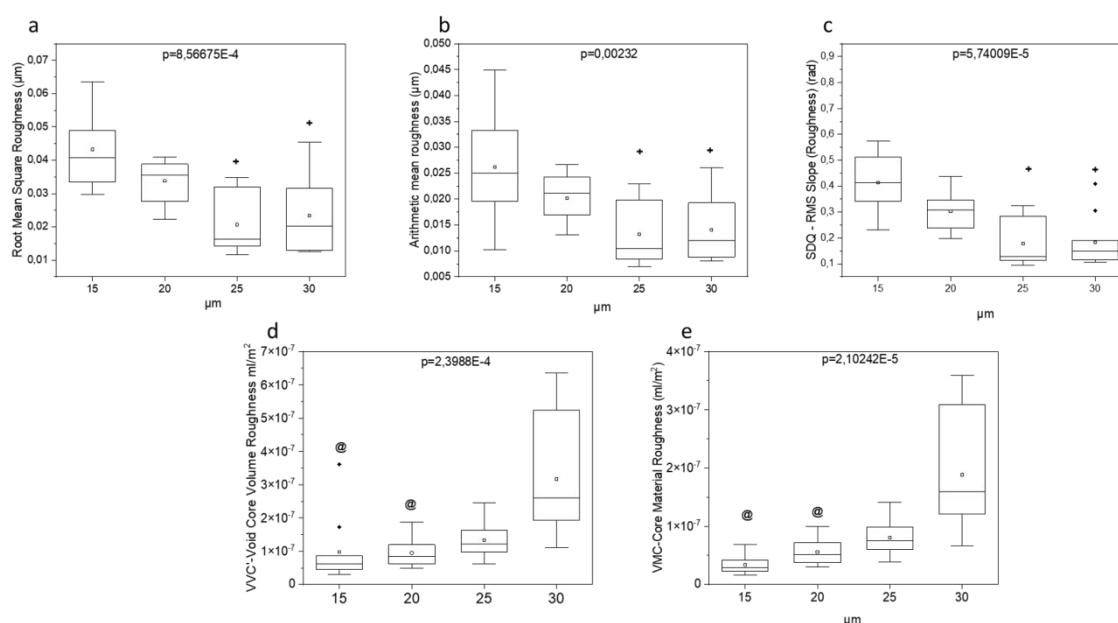


Figure 6. Surface analysis of HUVEC (a) Root mean square roughness; (b) Arithmetic mean roughness; (c) Root mean slope roughness; (d)VMC – Core material roughness; (e) VVC' Void Core Volume Roughness. Statistical analysis and graphs are made with Kruskal-Wallis ANOVA followed by Dunn's test for multiple comparisons (OriginPro) with * $p < 0.05$ versus 15 μ m and $^s p < 0.05$ versus 20 μ m and $^@ p < 0.05$ versus 30 μ m.

1
2
3 These data suggest that the 30 μm patterned cells exhibit a flatter surface with a slow increase
4
5 in height, an overall lower profile, and a surface roughness comparable to most other
6
7 distributions but less steep, as suggested by the Sdq measurements (**Error! Reference source not**
8
9 **found.** c and Figure 6 c). The 25 μm surfaces share similar characteristics in height, roughness,
10
11 and slope but significantly differ in terms of height distribution and surface volume distribution
12
13 (Figure 5 a and b; Figure 6 d). These results suggest that the 30 μm patterned cells, while mostly
14
15 flat, contains some small and steep elements that simultaneously produce a height distribution
16
17 with a longer right tail with high skewness (**Error! Reference source not found.** a) and highly
18
19 leptokurtotic profile (**Error! Reference source not found.** b).

26 Conclusion

27
28
29
30 This study posed itself the goal to enhance the reproducibility and accuracy of AFM
31
32 measurements of single-cell topography through micropatterning, by imposing a regular, square
33
34 geometry on the substrate. Our results indicate that endothelial cells cultured on micropatterned
35
36 surfaces adopt a morphology that facilitates the extraction of key topographical parameters such
37
38 as average and RMS height, slope (Sdq), maximum peak height, as well as statistical descriptors
39
40 like skewness and kurtosis. Notably, we observed that a reduction in available surface area
41
42 induces a significant increase in both the average and RMS height, with a clear differentiation
43
44 between cells patterned 15 μm square surfaces compared to those cultured on bigger patterns
45
46 (25–30 μm square). Moreover, cells on the largest pattern (e.g., 30 μm) exhibited a markedly
47
48 higher kurtosis and skewness, suggesting a more concentrated height distribution with a
49
50 pronounced right tail, likely reflecting the presence of sharp, steep features against a generally
51
52 flat base. The integration of high-pass filtering further enabled us to isolate the high-frequency
53
54
55
56
57
58
59
60

1
2
3 components of surface roughness, allowing for a full cell measurement of membrane rugosity
4
5 and texture. Collectively, these findings not only validate the use of micropatterning as a means
6
7 to standardize cell shape and improve measurement precision but also underscore its potential
8
9 to uncover subtle variations in cell mechanics and morphology that may have important
10
11 biological implications. Future studies should focus on further investigating how additional
12
13 factors might impact topographical characteristics, including the micropatterning technique
14
15 used, the type of substrate and its mechanical properties, or the methods employed for sample
16
17 fixation and drying prior to experimentation.
18
19
20
21
22

23 AUTHOR INFORMATION

24 **Corresponding Authors**

25
26
27 Daniele PEDRONI : daniele.pedroni@univ-lorraine.fr
28
29

30
31
32 Halima ALEM : halima.alem@univ-lorraine.fr
33
34

35 **Author Contributions**

36
37
38 The manuscript was written through contributions of all authors. All authors have given
39
40 approval to the final version of the manuscript.
41
42
43
44
45

46 **Acknowledgments**

47
48 The work was supported by the French PIA project “Lorraine Université d’Excellence”
49
50 reference ANR-15-IDEX-04-LUE. We are Thankfull to the CC Minalor platformfor their help
51
52 and their advices.
53
54
55

56 ABBREVIATIONS

57
58
59
60

1
2
3 HUVECs Human umbilical vein endothelial cells; AFM Atomic Force Microscopy; PEG
4
5 polyethylene glycol; PBS phosphate buffered saline; NCM Non-Contact Mode; AUC Area
6
7
8 Under Curve; RMS Root mean Square; Sq RMS height; Sa arithmetic mean height; Sku
9
10 kurtosis; Ssk skewness; Sk maximum height of the peaks; Sdq root mean square slope; VVC'
11
12
13 Void core volume; VMC' core material volume
14
15
16
17
18
19
20
21
22
23
24

25 References

- 26 1. Binnig, G., Quate, C. F. & Gerber, C. Atomic Force Microscope. in *Scanning Tunneling*
27
28 *Microscopy* (ed. Neddermeyer, H.) vol. 6 55–58 (Springer Netherlands, Dordrecht, 1993).
29
30
- 31 2. Buscarino, G. Atomic Force Microscopy and Spectroscopy. in *Spectroscopy for*
32
33 *Materials Characterization* (ed. Agnello, S.) 425–460 (Wiley, 2021).
34
35 doi:10.1002/9781119698029.ch15.
36
37
38
- 39 3. Vahabi, S., Nazemi Salman, B. & Javanmard, A. Atomic force microscopy application
40
41 in biological research: a review study. *Iran J Med Sci* **38**, 76–83 (2013).
42
43
44
- 45 4. Kontomaris, S. V. & Stylianou, A. Atomic force microscopy for university students:
46
47 applications in biomaterials. *Eur. J. Phys.* **38**, 033003 (2017).
48
49
50
- 51 5. Firtel, M., Henderson, G. & Sokolov, I. Nanosurgery: observation of peptidoglycan
52
53 strands in *Lactobacillus helveticus* cell walls. *Ultramicroscopy* **101**, 105–109 (2004).
54
55
56
57
58
59
60

- 1
2
3 6. Muller, D. J. AFM: A Nanotool in Membrane Biology. *Biochemistry* **47**, 7986–7998
4
5
6 (2008).
7
- 8
9 7. Li, M., Dang, D., Liu, L., Xi, N. & Wang, Y. Atomic Force Microscopy in
10
11
12
13
14
15
16
17
18
19
20
21
22
23
24
25
26
27
28
29
30
31
32
33
34
35
36
37
38
39
40
41
42
43
44
45
46
47
48
49
50
51
52
53
54
55
56
57
58
59
60
61
62
63
64
65
66
67
68
69
70
71
72
73
74
75
76
77
78
79
80
81
82
83
84
85
86
87
88
89
90
91
92
93
94
95
96
97
98
99
100
101
102
103
104
105
106
107
108
109
110
111
112
113
114
115
116
117
118
119
120
121
122
123
124
125
126
127
128
129
130
131
132
133
134
135
136
137
138
139
140
141
142
143
144
145
146
147
148
149
150
151
152
153
154
155
156
157
158
159
160
161
162
163
164
165
166
167
168
169
170
171
172
173
174
175
176
177
178
179
180
181
182
183
184
185
186
187
188
189
190
191
192
193
194
195
196
197
198
199
200
201
202
203
204
205
206
207
208
209
210
211
212
213
214
215
216
217
218
219
220
221
222
223
224
225
226
227
228
229
230
231
232
233
234
235
236
237
238
239
240
241
242
243
244
245
246
247
248
249
250
251
252
253
254
255
256
257
258
259
260
261
262
263
264
265
266
267
268
269
270
271
272
273
274
275
276
277
278
279
280
281
282
283
284
285
286
287
288
289
290
291
292
293
294
295
296
297
298
299
300
301
302
303
304
305
306
307
308
309
310
311
312
313
314
315
316
317
318
319
320
321
322
323
324
325
326
327
328
329
330
331
332
333
334
335
336
337
338
339
340
341
342
343
344
345
346
347
348
349
350
351
352
353
354
355
356
357
358
359
360
361
362
363
364
365
366
367
368
369
370
371
372
373
374
375
376
377
378
379
380
381
382
383
384
385
386
387
388
389
390
391
392
393
394
395
396
397
398
399
400
401
402
403
404
405
406
407
408
409
410
411
412
413
414
415
416
417
418
419
420
421
422
423
424
425
426
427
428
429
430
431
432
433
434
435
436
437
438
439
440
441
442
443
444
445
446
447
448
449
450
451
452
453
454
455
456
457
458
459
460
461
462
463
464
465
466
467
468
469
470
471
472
473
474
475
476
477
478
479
480
481
482
483
484
485
486
487
488
489
490
491
492
493
494
495
496
497
498
499
500
501
502
503
504
505
506
507
508
509
510
511
512
513
514
515
516
517
518
519
520
521
522
523
524
525
526
527
528
529
530
531
532
533
534
535
536
537
538
539
540
541
542
543
544
545
546
547
548
549
550
551
552
553
554
555
556
557
558
559
560
561
562
563
564
565
566
567
568
569
570
571
572
573
574
575
576
577
578
579
580
581
582
583
584
585
586
587
588
589
590
591
592
593
594
595
596
597
598
599
600
601
602
603
604
605
606
607
608
609
610
611
612
613
614
615
616
617
618
619
620
621
622
623
624
625
626
627
628
629
630
631
632
633
634
635
636
637
638
639
640
641
642
643
644
645
646
647
648
649
650
651
652
653
654
655
656
657
658
659
660
661
662
663
664
665
666
667
668
669
670
671
672
673
674
675
676
677
678
679
680
681
682
683
684
685
686
687
688
689
690
691
692
693
694
695
696
697
698
699
700
701
702
703
704
705
706
707
708
709
710
711
712
713
714
715
716
717
718
719
720
721
722
723
724
725
726
727
728
729
730
731
732
733
734
735
736
737
738
739
740
741
742
743
744
745
746
747
748
749
750
751
752
753
754
755
756
757
758
759
760
761
762
763
764
765
766
767
768
769
770
771
772
773
774
775
776
777
778
779
780
781
782
783
784
785
786
787
788
789
790
791
792
793
794
795
796
797
798
799
800
801
802
803
804
805
806
807
808
809
810
811
812
813
814
815
816
817
818
819
820
821
822
823
824
825
826
827
828
829
830
831
832
833
834
835
836
837
838
839
840
841
842
843
844
845
846
847
848
849
850
851
852
853
854
855
856
857
858
859
860
861
862
863
864
865
866
867
868
869
870
871
872
873
874
875
876
877
878
879
880
881
882
883
884
885
886
887
888
889
890
891
892
893
894
895
896
897
898
899
900
901
902
903
904
905
906
907
908
909
910
911
912
913
914
915
916
917
918
919
920
921
922
923
924
925
926
927
928
929
930
931
932
933
934
935
936
937
938
939
940
941
942
943
944
945
946
947
948
949
950
951
952
953
954
955
956
957
958
959
960
961
962
963
964
965
966
967
968
969
970
971
972
973
974
975
976
977
978
979
980
981
982
983
984
985
986
987
988
989
990
991
992
993
994
995
996
997
998
999
1000
8. Rianna, C. & Radmacher, M. Cell mechanics as a marker for diseases: Biomedical applications of AFM. in 020057 (Tomsk, Russia, 2016). doi:10.1063/1.4960276.
9. Kasas, S., Longo, G. & Dietler, G. Mechanical properties of biological specimens explored by atomic force microscopy. *J. Phys. D: Appl. Phys.* **46**, 133001 (2013).
10. Mingeot-Leclercq, M.-P., Deleu, M., Brasseur, R. & Dufrêne, Y. F. Atomic force microscopy of supported lipid bilayers. *Nat Protoc* **3**, 1654–1659 (2008).
11. Li, G., Xi, N. & Wang, D. H. Probing membrane proteins using atomic force microscopy. *J Cell Biochem* **97**, 1191–1197 (2006).
12. Haupt, B. J., Pelling, A. E. & Horton, M. A. Integrated Confocal and Scanning Probe Microscopy for Biomedical Research. *The Scientific World JOURNAL* **6**, 1609–1618 (2006).
13. Lehenkari, P. P. & Horton, M. A. Single Integrin Molecule Adhesion Forces in Intact Cells Measured by Atomic Force Microscopy. *Biochemical and Biophysical Research Communications* **259**, 645–650 (1999).

- 1
2
3 14. Shroff, S. G., Saner, D. R. & Lal, R. Dynamic micromechanical properties of cultured
4
5 rat atrial myocytes measured by atomic force microscopy. *American Journal of Physiology-*
6
7 *Cell Physiology* **269**, C286–C292 (1995).
8
9
- 10
11 15. Haga, H. *et al.* Elasticity mapping of living fibroblasts by AFM and
12
13 immunofluorescence observation of the cytoskeleton. *Ultramicroscopy* **82**, 253–258 (2000).
14
15
- 16
17 16. Boitor, R., Sinjab, F., Strohbuecker, S., Sottile, V. & Notingher, I. Towards quantitative
18
19 molecular mapping of cells by Raman microscopy: using AFM for decoupling molecular
20
21 concentration and cell topography. *Faraday Discuss.* **187**, 199–212 (2016).
22
23
- 24
25 17. Cascione, M., De Matteis, V., Rinaldi, R. & Leporatti, S. Atomic force microscopy
26
27 combined with optical microscopy for cells investigation. *Microscopy Res & Technique* **80**,
28
29 109–123 (2017).
30
31
- 32
33 18. Ding, L., Wendl, M. C., McMichael, J. F. & Raphael, B. J. Expanding the computational
34
35 toolbox for mining cancer genomes. *Nat Rev Genet* **15**, 556–570 (2014).
36
37
- 38
39 19. Blainey, P. C. & Quake, S. R. Dissecting genomic diversity, one cell at a time. *Nat*
40
41 *Methods* **11**, 19–21 (2014).
42
43
- 44
45 20. Van Loo, P. & Voet, T. Single cell analysis of cancer genomes. *Current Opinion in*
46
47 *Genetics & Development* **24**, 82–91 (2014).
48
49
- 50
51 21. Lulevich, V., Zink, T., Chen, H.-Y., Liu, F.-T. & Liu, G. Cell Mechanics Using Atomic
52
53 Force Microscopy-Based Single-Cell Compression. *Langmuir* **22**, 8151–8155 (2006).
54
55
56
57
58
59
60

1
2
3 22. Lekka, M. & Pabijan, J. Measuring Elastic Properties of Single Cancer Cells by AFM.
4
5 in *Atomic Force Microscopy* (eds. Santos, N. C. & Carvalho, F. A.) vol. 1886 315–324
6
7 (Springer New York, New York, NY, 2019).
8
9

10
11 23. Hohmann, T. & Dehghani, F. Measuring Mechanical and Adhesive Properties of Single
12
13 Cells Using an Atomic Force Microscope. in *Metastasis* (ed. Stein, U. S.) vol. 2294 81–92
14
15 (Springer US, New York, NY, 2021).
16
17
18

19
20 24. Zhou, X. *et al.* Reversed cell imprinting, AFM imaging and adhesion analyses of cells
21
22 on patterned surfaces. *Lab Chip* **10**, 1182 (2010).
23
24
25

26 25. Gross, A. *et al.* Technologies for Single-Cell Isolation. *IJMS* **16**, 16897–16919 (2015).
27
28

29
30 26. Karimian, T., Hager, R., Karner, A., Weghuber, J. & Lanzerstorfer, P. A Simplified and
31
32 Robust Activation Procedure of Glass Surfaces for Printing Proteins and Subcellular
33
34 Micropatterning Experiments. *Biosensors* **12**, 140 (2022).
35
36
37

38 27. Nishizawa, M., Takoh, K. & Matsue, T. Micropatterning of HeLa Cells on Glass
39
40 Substrates and Evaluation of Respiratory Activity Using Microelectrodes. *Langmuir* **18**, 3645–
41
42 3649 (2002).
43
44
45

46
47 28. Bautista, M., Fernandez, A. & Pinaud, F. A Micropatterning Strategy to Study Nuclear
48
49 Mechanotransduction in Cells. *Micromachines* **10**, 810 (2019).
50
51

52
53 29. Gao, D., Kumar, G., Co, C. & Ho, C.-C. Formation of Capillary Tube-like Structures
54
55 on Micropatterned Biomaterials. in *Oxygen Transport to Tissue XXIX* (eds. Kang, K. A.,
56
57 Harrison, D. K. & Bruley, D. F.) vol. 614 199–205 (Springer US, Boston, MA, 2008).
58
59
60

1
2
3 30. Badv, M., Imani, S. M., Weitz, J. I. & Didar, T. F. Lubricant-Infused Surfaces with
4 Built-In Functional Biomolecules Exhibit Simultaneous Repellency and Tunable Cell
5 Adhesion. *ACS Nano* **12**, 10890–10902 (2018).
6
7
8
9

10
11 31. Noiri, M. *et al.* Influence of cell adhesive molecules attached onto PEG-lipid-modified
12 fluid surfaces on cell adhesion. *Colloids and Surfaces B: Biointerfaces* **175**, 375–383 (2019).
13
14
15
16

17 32. Saneinejad, S. & Shoichet, M. S. Patterned glass surfaces direct cell adhesion and
18 process outgrowth of primary neurons of the central nervous system. *J. Biomed. Mater. Res.*
19 **42**, 13–19 (1998).
20
21
22
23
24
25

26 33. Azioune, A., Storch, M., Bornens, M., Théry, M. & Piel, M. Simple and rapid process
27 for single cell micro-patterning. *Lab Chip* **9**, 1640 (2009).
28
29
30
31

32 34. Fink, J. *et al.* Comparative study and improvement of current cell micro-patterning
33 techniques. *Lab Chip* **7**, 672–680 (2007).
34
35
36
37

38 35. Pallandre, A., Glinel, K., Jonas, A. M. & Nysten, B. Binary Nanopatterned Surfaces
39 Prepared from Silane Monolayers. *Nano Lett.* **4**, 365–371 (2004).
40
41
42
43

44 36. Kim, D. J., Lee, J. M., Park, J. & Chung, B. G. A self-assembled monolayer-based
45 micropatterned array for controlling cell adhesion and protein adsorption. *Biotech &*
46 *Bioengineering* **108**, 1194–1202 (2011).
47
48
49
50
51

52 37. Dirscherl, C. & Springer, S. Protein micropatterns printed on glass: Novel tools for
53 protein-ligand binding assays in live cells. *Engineering in Life Sciences* **18**, 124–131 (2018).
54
55
56
57
58
59
60

- 1
2
3 38. Chen, C. S., Mrksich, M., Huang, S., Whitesides, G. M. & Ingber, D. E. Micropatterned
4 Surfaces for Control of Cell Shape, Position, and Function. *Biotechnol. Prog.* **14**, 356–363
5
6 (1998).
7
8
9
10
11 39. Chen, C. S., Mrksich, M., Huang, S., Whitesides, G. M. & Ingber, D. E. Geometric
12 Control of Cell Life and Death. *Science* **276**, 1425–1428 (1997).
13
14
15
16
17 40. Sato, M., Levesque, M. J. & Nerem, R. M. Micropipette aspiration of cultured bovine
18 aortic endothelial cells exposed to shear stress. *Arteriosclerosis* **7**, 276–286 (1987).
19
20
21
22
23 41. Gray, D. S. *et al.* Engineering amount of cell-cell contact demonstrates biphasic
24 proliferative regulation through RhoA and the actin cytoskeleton. *Exp Cell Res* **314**, 2846–2854
25
26 (2008).
27
28
29
30
31 42. Pedroni, D., Gaucher, C., Ba, D., Badie, L., Raeth-Fries, I. & Halima, A. *Advanced*
32 *Engineering Materials - under review*
33
34
35
36
37
38
39
40
41
42 43. *Machining and Tribology*. (Elsevier, 2022). doi:10.1016/C2019-0-00230-0.
43
44
45 44. Kolodziej, C. M. & Maynard, H. D. Electron-Beam Lithography for Patterning
46 Biomolecules at the Micron and Nanometer Scale. *Chem. Mater.* **24**, 774–780 (2012).
47
48
49
50
51 45. McMurray, R., J, M. & Gadegaar, N. Nanopatterned Surfaces for Biomedical
52 Applications. in *Biomedical Engineering, Trends in Materials Science* (ed. Laskovski, A.)
53
54 (InTech, 2011). doi:10.5772/13453.
55
56
57
58
59
60

1
2
3 46. Kolodziej, C. M. *et al.* Combination of Integrin-Binding Peptide and Growth Factor
4 Promotes Cell Adhesion on Electron-Beam-Fabricated Patterns. *J. Am. Chem. Soc.* **134**, 247–
5 255 (2012).
6
7
8
9

10
11 47. Ermis, M., Antmen, E. & Hasirci, V. Micro and Nanofabrication methods to control
12 cell-substrate interactions and cell behavior: A review from the tissue engineering perspective.
13
14
15
16
17 *Bioact Mater* **3**, 355–369 (2018).
18
19

20 48. Samantaray, C. B. & Hastings, J. T. The effect of thin metal overlayers on the electron
21 beam exposure of polymethyl methacrylate. *Journal of Vacuum Science & Technology B:*
22
23 *Microelectronics and Nanometer Structures Processing, Measurement, and Phenomena* **26**,
24
25 2300–2305 (2008).
26
27
28
29

30 49. Segerer, F. J. *et al.* Versatile method to generate multiple types of micropatterns.
31
32
33 *Biointerphases* **11**, 011005 (2016).
34
35
36

37 50. Wu, C.-C. *et al.* Directional shear flow and Rho activation prevent the endothelial cell
38 apoptosis induced by micropatterned anisotropic geometry. *Proc. Natl. Acad. Sci. U.S.A.* **104**,
39
40 1254–1259 (2007).
41
42
43
44

45 51. Kam, L. & Boxer, S. G. Cell adhesion to protein-micropatterned-supported lipid bilayer
46 membranes. *J Biomed Mater Res* **55**, 487–495 (2001).
47
48
49

50 52. Pollice, A. A. *et al.* Sequential paraformaldehyde and methanol fixation for
51 simultaneous flow cytometric analysis of DNA, cell surface proteins, and intracellular proteins.
52
53
54
55
56
57 *Cytometry* **13**, 432–444 (1992).
58
59
60

- 1
2
3 53. Mufson, E. J., Perez, S. E., Kelley, C. M., Alldred, M. J. & Ginsberg, S. D. Fixation
4
5
6 Protocols for Neurohistology: Neurons to Genes. in *Neurohistology and Imaging Techniques*
7
8 (eds. Pelc, R., Walz, W. & Doucette, J. R.) vol. 153 49–71 (Springer US, New York, NY, 2020).
9
10
11
12 54. Smit, J. W., Meijer, C. J. L. M., Decary, F. & Feltkamp-vroom, T. M. Paraformaldehyde
13
14 fixation in immunofluorescence and immunoelectron microscopy. *Journal of Immunological*
15
16 *Methods* **6**, 93–98 (1974).
17
18
19
20 55. Osorio, E., Toledano, M., Aguilera, F. S., Tay, F. R. & Osorio, R. Ethanol Wet-bonding
21
22 Technique Sensitivity Assessed by AFM. *J Dent Res* **89**, 1264–1269 (2010).
23
24
25
26 56. Weber, A., Iturri, J., Benitez, R., Zemljic-Jokhadar, S. & Toca-Herrera, J. L.
27
28 Microtubule disruption changes endothelial cell mechanics and adhesion. *Sci Rep* **9**, 14903
29
30 (2019).
31
32
33
34
35 57. Wu, Y. *et al.* The analysis of morphological distortion during AFM study of cells.
36
37 *Scanning* **30**, 426–432 (2008).
38
39
40
41 58. Hecht, E. *et al.* Combined Atomic Force Microscopy–Fluorescence Microscopy:
42
43 Analyzing Exocytosis in Alveolar Type II Cells. *Anal. Chem.* **84**, 5716–5722 (2012).
44
45
46
47 59. Docheva, D. *et al.* Researching into the cellular shape, volume and elasticity of
48
49 mesenchymal stem cells, osteoblasts and osteosarcoma cells by atomic force microscopy. *J*
50
51 *Cellular Molecular Medi* **12**, 537–552 (2008).
52
53
54
55
56
57
58
59
60

- 1
2
3 60. Wang, D.-C., Chen, K.-Y., Tsai, C.-H., Chen, G.-Y. & Chen, C.-H. AFM membrane
4 roughness as a probe to identify oxidative stress-induced cellular apoptosis. *Journal of*
5
6 *Biomechanics* **44**, 2790–2794 (2011).
7
8
9
10
11 61. Lee, C.-W. *et al.* Membrane roughness as a sensitive parameter reflecting the status of
12 neuronal cells in response to chemical and nanoparticle treatments. *J Nanobiotechnol* **14**, 9
13
14 (2016).
15
16
17
18
19 62. D Antonio, P., Lasalvia, M., Perna, G. & Capozzi, V. Scale-independent roughness
20 value of cell membranes studied by means of AFM technique. *Biochimica et Biophysica Acta*
21
22 *(BBA) - Biomembranes* **1818**, 3141–3148 (2012).
23
24
25
26
27
28 63. Chang, C.-H., Lee, H.-H. & Lee, C.-H. Substrate properties modulate cell membrane
29 roughness by way of actin filaments. *Sci Rep* **7**, 9068 (2017).
30
31
32
33
34
35
36
37
38
39
40
41
42
43
44
45
46
47
48
49
50
51
52
53
54
55
56
57
58
59
60